Comprehending the Single-Electron Reactivity of First-Row Transition Metals – a Computational Group 10 Case Study

JD Rolfes

Albert Hofmann Institute for Physiochemical Sustainability, Albert-Schweitzer-Str. 22, D–32602 Vlotho, Germany.
Contact: jd.rolfes@a-h.institute

The reactivity and structural properties of transition metals and their compounds depend on the electronic configuration of the *d* orbitals, specifically the valence *d* orbitals. First-row transition metals are generally more prone to single-electron chemistry than second- or third-row transition metals. This study presents a computational investigation of group 10 transition metals, focusing on their potential energy surfaces and specific electronic properties. Theoretical X-ray emission spectroscopy was employed to analyze potential electronic transitions from valence-d_{xy} orbitals to the 1*s* orbitals of the metal centers. Our findings suggest that the spin polarization of 3*d* orbitals in first-row transition metals may play a crucial role in their single-electron reactivity, offering a potential explanation for the observed differences in reactivity between 3*d*, 4*d*, and 5*d* elements. This study represents a first step towards a generalized description of valence electron spin polarizability, including elemental parametrization.

Introduction

The reactivity and structural properties of transition metals and their compounds depend, among other factors, on the electronic configuration of the *d* orbitals, specifically the valence *d* orbitals. Interestingly, first-row transition metals are observed to be generally more prone to single electron chemistry than second or third-row transition metals. [1-4] More data in alignment of this observation was recently brought by a series of findings from the Ritter group (Fig. 1): [5, 6] an organometallic group-10 valence-d^8 complex was fluoro-oxidized to perform a reductive elimination, yielding a fluoroarene. Interestingly, the group found out that the Ni complex reacts *via* reactive intermediate with a $3d^7$ shell occupation including an unpaired electron, [7] and the Pd complex *via* $4d^6$ closed-shell intermediate, performing 2-electron chemistry. [8]

Spin Polarization is normally defined as $P = (T+ - T-) / (T+ + T-)$, with $T\pm$ as the amplitude of the incident and outgoing wave amplitudes, which are scalar coefficients. [9] It is the degree to which spin is aligned with a given direction. [10] Alignment of spin with an external magnetic field is the basis of NMR and EPR spectroscopy. [11] However, spin polarization can also be observed as an intra-structural phenomenon. [12] In molecular systems with more than one unpaired electron, a dynamic spin polarization is observed, depending on the relative spin orientation of the unpaired electrons. [13] The presence of unpaired spin in molecules can induce tunable spin polarization and also affect bond orders in radicals. [14, 15] Jørgensen's parametrization of spin pairing energy helped facilitating computation of spin states, especially for the transition metals and lanthanides. [16-18] More recent publications discuss the improvement of computations for open-shell systems, including the evaluation of spin density

distributions and spin polarization effects. [19-22] Spin polarization in chiral molecules has also been explored [23, 24] and the field of spintronics, concerning spin-charge coupling in metallic systems, is long described. [25-28]

X-ray spectroscopy is a fundamental experimental tool to gain insight into the geometric and electronic structure of inorganic systems. [29] X-ray emission spectroscopy (XES) is an element-specific method for studying the electronic structure of materials and was originally developed in 1882 by Henry Rowland for the optical wavelength range, using spherical concave gratings to focus light. [30, 31] In XES, the emission of photons is followed by the decay of electrons after the ionization of the 1*s* electron of the metal. [29] Valence-to-core X-ray emission spectroscopy (V2C XES) is a type of XES that measures the energy of emitted photons following the decay of valence electrons with a spectral resolution sufficient to analyze the impact of the chemical environment on the photon emission. [32-34] Dependence of V2C XES energies on the spin of the ionized 1s electrons in open-shell complexes is an open field of investigation. [35]

Levels of Theory

All computations were performed with the ORCA program package. [36, 37] Geometries were optimized at (PBE0-D3/def2-TZVP) level. [38-44] Single point energies were calculated at (CPCM(MeCN) DLPNO-CCSD(T)/DKH2/SARC-DKH-TZVPP[Pd+Pt]/DKH-def2-TZVPP) level. [39, 45-60] X-ray emission spectra were generated at (PBE0-D3/DKH2/SARC-DKH-TZVP[Pd+Pt]/DKH-def2-TZVP) level. [38-44, 50-59] The Avogadro program was used for generation of starting geometries as well as analysis and visualization of computation results. [61] Further details on the computations, including coordinates of all geometries and single point energies, can be found in the Supporting Information.

Equilibrium constants K_{eq} were calculated from the equilibrium energies at T = 293.15 K:

$$K_{eq} = \exp\left(\Delta G_{eq}/-RT\right) \quad (1)$$

Results

A model reaction system was set up, as shown in Fig. 1, that was optimized for computation, while still in close alignment with the systems used in practice by Ritter et al. [5-8] The present investigation focused on the potential energy surface (PES) and specific electronic properties of the molecules, namely potential electronic transitions from valence-d_{xy} orbitals to the 1*s* orbitals of the metal centers, by theoretical *X-ray emission spectroscopy* (XES).

Starting with the partial analysis of the potential energy surface (PES) of the active intermediates including the consecutive C–F reductive eliminations of all Group 10 analogs of the reaction depicted in Fig. 1, the center of consideration is the equilibrium of the active intermediates in the center of the equations. The calculated Gibbs Free Energies of the equilibrium reaction, as well as the activation barriers and the Gibbs Free Energies of the reductive eliminations from the active intermediates of both oxidation states, III and IV, as shown in Fig. 1, for all three Group 10 elements; Nickel, Palladium, and Platinum; are depicted in Fig. 2c and written out in Tab. 1, together with the equilibrium constants K_{eq}.

For the calculation of the XES energies of the [valence]$d_{xy} \rightarrow 1s$ transition in the active intermediates, the corresponding orbitals were determined based on *Loewdin Reduced Orbital Population per MO* analysis. The visualizations of the d_{xy} orbitals with *iso* values of 0.2 and 0.1 can be found in the Supporting Information.

Discussion

First and foremost, based on the calculations, all considered reaction paths are interpretable as feasible in principle, within the reported reaction conditions. For the central equilibrium, the closed-shell oxidation state IV is preferred for Pd and Pt, whereas the open-shell oxidation state III is preferred for Ni. Hence, the calculations are in alignment with the experimental observations. The comparison of the activation barriers of the reductive eliminations supports these findings further, as only for Ni the barrier of the reductive elimination from [M(III)–F] is lower than the barrier of the reductive elimination from [M(IV)–F], taken into account the equilibrium distribution.

Although the reductive elimination from [M(III)–F] itself is (at least for the model system) an endothermal reaction, the [M(I)–MeCN] product of the reductive elimination from [M(III)–F] will react further, as reported. The reaction is thus pulled towards the endothermal product of the reductive elimination, making a utilization of the Ni complex as a catalyst impossible. For Pd and Pt, a different observation can be made: As shown experimentally at least for the Pd complex, they can be used catalytically, which is supported by the findings that the reductive elimination from [M(IV)–F] is generally an exothermal reaction. The resulting [M(II)–MeCN] complex proves to be stable enough for re-activation through substrate addition and oxidation to the active intermediate [M(IV)–F]. The high activation barriers of the reactions with the Pt complexes give a potential explanation for the fact that the reaction was so far only reported with Ni and Pd as active centers.

Probably the most interesting finding presented herein is the energy difference of the alpha and beta transitions, reported in Table 2: the surprisingly strong spin polarization of the [Ni(III)–F] complex offers a potential explanation for the preferred reaction path, and more general, a potential explanation for the fact that 3*d* elements are more prone to single-electron chemistry than the 4*d* and 5*d* elements. Assuming that the spin-polarization of the 1*s* orbital is neglectable, due to its extreme proximity to the core, the difference in alpha and beta transition can be almost completely attributed to the spin polarization of the $3d_{xy}$ orbital. In Pd and Pt, only very weak spin polarization can be observed, whereas in Ni, observable spin polarization is substantially.

This "flexibility" of the 3*d* orbitals over the 4*d* and 5*d* orbitals has the potential to explain the general stabilization of the open-shell complexes that are a necessary part in single-electron reactions: the energy of the unpaired electron is buffered further by the stronger spin polarization it exerts. A potential reason for these differences in flexibility can be the fact that the 3*d* orbitals are the innermost *d* orbitals. For 4*d* and 5*d* occupation, at least one inner *d* shell is fully occupied, potentially adding rigidity to the valence *d* orbitals.

The considered reaction path shown in Fig. 1 is a plausible, but not necessarily the most probable reaction route. For the Pd system, Ritter et al. reported a slightly different ligand positioning in the mechanistic analysis, and for the Ni system, the specific system considered here was never

reported. However, for the purpose of comparability, we decided to focus on this specific reaction path. A full PES analysis was not conducted.

The XES transitions reported in Tab. 2 have an extremely low intensity. Most likely, they will not be observable experimentally. A major challenge for future investigations, potentially validating the computed data experimentally, is the design of a system with the relevant transitions in a detectable intensity range.

Conclusion

In conclusion, this computational study on group 10 transition metals has given a feasible explanation for the reaction patterns experimentally observed by the Ritter group, and provided preliminary insights into the single-electron reactivity of first-row transition metals. Further research is needed to determine if the finding described above is exclusive to group 10 elements, maybe even to the model system analyzed herein, or if it turns out to be a general trend among the transition metals.

A more comprehensive investigation into the spin polarization of late transition metals at high levels of theory is necessary to better understand the general character of the findings described in this study. A first attempt to map and parametrize the spin polarization for all late transition metals on Hartree-Fock level of theory can be found in the Supporting Information. However, due to the poor level of theory, including the possibility of just calculating spin contamination, confidence in the parameters is extremely low. The purpose of the analysis appended in the Supporting Information is to deliver a starting point for the investigation into the general character of the findings described herein.

Acknowledgements

Support by Akademie zur Förderung physiochemischer Nachhaltigkeit and the Max-Planck-Institut für Kohlenforschung is gratefully acknowledged. The author wants to thank Frank Neese, Maurice van Gastel, Zachary Mathe, Giovanni Bistoni, Mihail Atanasov, Dimitrios A. Pantazis, Penelope Pesara, and Tobias Ritter for their input and fruitful discussions.

Supporting Information. A detailed description of the calculation methods, cartesian coordinates of all geometry optimized model structures including electronic energies and thermal corrections to Gibbs Free Energy, visualizations of the d_{xy}-type MOs, and a first parametrization of spin polarization for the late transition metals on Hartree-Fock level of theory are supplied as Supporting Information.

Conflict of Interest. The authors declare no conflict of interest.

References

[1] Nicholls, D., *Introduction to the First-row Transition Elements*, in *Complexes and First-Row Transition Elements*, D. Nicholls, Editor. 1974, Macmillan Education UK: London. p. 120-127.
[2] McCleverty, J., *Chemistry of the First-row Transition Metals*. Oxford Chemistry Primers. 1999, Oxford: Oxford University Press.
[3] Smith, K.M., *Single Electron Transfer Reactions in the Synthetic Organometallic Chemistry of First-Row Transition Metals.* Organometallics, 2005. **24**(5): p. 778-784.

[4] Van Cleave, C. and D.C. Crans, *The First-Row Transition Metals in the Periodic Table of Medicine.* Inorganics, 2019. **7**(9): p. 111.
[5] Furuya, T. and T. Ritter, *Carbon-fluorine reductive elimination from a high-valent palladium fluoride.* J Am Chem Soc, 2008. **130**(31): p. 10060-1.
[6] Lee, E., J.M. Hooker, and T. Ritter, *Nickel-mediated oxidative fluorination for PET with aqueous [18F] fluoride.* J Am Chem Soc, 2012. **134**(42): p. 17456-8.
[7] Lee, H., J. Börgel, and T. Ritter, *Carbon-Fluorine Reductive Elimination from Nickel(III) Complexes.* Angew Chem Int Ed Engl, 2017. **56**(24): p. 6966-6969.
[8] Furuya, T., et al., *Mechanism of C-F reductive elimination from palladium(IV) fluorides.* J Am Chem Soc, 2010. **132**(11): p. 3793-807.
[9] Tan, S.G. and M.B.A. Jalil, *5 - Spintronics and spin Hall effects in nanoelectronics*, in *Introduction to the Physics of Nanoelectronics*, S.G. Tan and M.B.A. Jalil, Editors. 2012, Woodhead Publishing. p. 141-197.
[10] Kessler, J., *Description of Polarized Electrons*, in *Polarized Electrons*, J. Kessler, Editor. 1976, Springer Berlin Heidelberg: Berlin, Heidelberg. p. 7-20.
[11] Kempe, S., H. Metz, and K. Mäder, *Application of Electron Paramagnetic Resonance (EPR) spectroscopy and imaging in drug delivery research – Chances and challenges.* European Journal of Pharmaceutics and Biopharmaceutics, 2010. **74**(1): p. 55-66.
[12] Lyons, T.P., et al., *The valley Zeeman effect in inter- and intra-valley trions in monolayer WSe2.* Nature Communications, 2019. **10**(1): p. 2330.
[13] Kollmar, H. and V. Staemmler, *Violation of Hund's rule by spin polarization in molecules.* Theoretica chimica acta, 1978. **48**(3): p. 223-239.
[14] Bajaj, A. and M.E. Ali, *Tuning of spin-polarized current in high spin organic molecules.* Physica B: Condensed Matter, 2020. **595**: p. 412396.
[15] Karafiloglou, P. and K. Kyriakidou, *Unpaired electrons, spin polarization, and bond orders in radicals from the 2-RDM in orbital spaces: Basic notions and testing calculations.* International Journal of Quantum Chemistry, 2014. **114**(11): p. 696-707.
[16] Jørgensen, C.K., *Refining the Parameters of the Refined Spin-Pairing Energy Description*, in *The Rare Earths in Modern Science and Technology: Volume 2*, G.J. McCarthy, J.J. Rhyne, and H.B. Silber, Editors. 1980, Springer US: Boston, MA. p. 425-428.
[17] Jørgensen, C.K., *New paradoxes of spin-pairing energy in gadolinium(III).* Journal of the Less Common Metals, 1989. **148**(1): p. 147-150.
[18] Jørgensen, C.K., R. Pappalardo, and H.H. Schmidtke, *Do the "Ligand Field" Parameters in Lanthanides Represent Weak Covalent Bonding?* The Journal of Chemical Physics, 1963. **39**(6): p. 1422-1430.
[19] Suaud, N., et al., *Singly Occupied MOs in Mono- and Diradical Conjugated Hydrocarbons: Comparison between Variational Single-Reference, π-Fully Correlated and Hückel Descriptions.* The Journal of Physical Chemistry A, 2014. **118**(31): p. 5876-5884.
[20] Giner, E. and C. Angeli, *Spin density and orbital optimization in open shell systems: A rational and computationally efficient proposal.* The Journal of Chemical Physics, 2016. **144**(10).
[21] David, G., et al., *Improved evaluation of spin-polarization energy contributions using broken-symmetry calculations.* The Journal of Chemical Physics, 2020. **153**(5).
[22] Stuyver, T., et al., *How Do Local Reactivity Descriptors Shape the Potential Energy Surface Associated with Chemical Reactions? The Valence Bond Delocalization Perspective.* Journal of the American Chemical Society, 2020. **142**(22): p. 10102-10113.
[23] Zhu, Q., et al., *Multistate Switching of Spin Selectivity in Electron Transport through Light-Driven Molecular Motors.* Advanced Science, 2021. **8**(18): p. 2101773.
[24] Fransson, J., *Charge Redistribution and Spin Polarization Driven by Correlation Induced Electron Exchange in Chiral Molecules.* Nano Letters, 2021. **21**(7): p. 3026-3032.
[25] Julliere, M., *Tunneling between ferromagnetic films.* Physics Letters A, 1975. **54**(3): p. 225-226.
[26] Johnson, M. and R.H. Silsbee, *Interfacial charge-spin coupling: Injection and detection of spin magnetization in metals.* Physical Review Letters, 1985. **55**(17): p. 1790-1793.

[27] Baibich, M.N., et al., *Giant Magnetoresistance of (001)Fe/(001)Cr Magnetic Superlattices.* Physical Review Letters, 1988. **61**(21): p. 2472-2475.
[28] Binasch, G., et al., *Enhanced magnetoresistance in layered magnetic structures with antiferromagnetic interlayer exchange.* Physical Review B, 1989. **39**(7): p. 4828-4830.
[29] DeBeer, S. and F. Neese, *9.16 - X-Ray Spectroscopy*, in *Comprehensive Inorganic Chemistry II (Second Edition)*, J. Reedijk and K. Poeppelmeier, Editors. 2013, Elsevier: Amsterdam. p. 427-439.
[30] Rowland, H.A., *LXI. Preliminary notice of the results accomplished in the manufacture and theory of gratings for optical purposes.* The London, Edinburgh, and Dublin Philosophical Magazine and Journal of Science, 1882. **13**(84): p. 469-474.
[31] Magnuson, M. and M. Mattesini, *Chemical bonding and electronic-structure in MAX phases as viewed by X-ray spectroscopy and density functional theory.* Thin Solid Films, 2017. **621**: p. 108-130.
[32] Delgado-Jaime, M.U., S. DeBeer , and M. Bauer, *Valence-to-Core X-Ray Emission Spectroscopy of Iron–Carbonyl Complexes: Implications for the Examination of Catalytic Intermediates.* Chemistry – A European Journal, 2013. **19**(47): p. 15888-15897.
[33] Bauer, M., *HERFD-XAS and valence-to-core-XES: new tools to push the limits in research with hard X-rays?* Physical Chemistry Chemical Physics, 2014. **16**(27): p. 13827-13837.
[34] MacMillan, S.N., et al., *Ligand-Sensitive But Not Ligand-Diagnostic: Evaluating Cr Valence-to-Core X-ray Emission Spectroscopy as a Probe of Inner-Sphere Coordination.* Inorganic Chemistry, 2015. **54**(1): p. 205-214.
[35] Geoghegan, B.L., et al., *Combining Valence-to-Core X-ray Emission and Cu K-edge X-ray Absorption Spectroscopies to Experimentally Assess Oxidation State in Organometallic Cu(I)/(II)/(III) Complexes.* Journal of the American Chemical Society, 2022. **144**(6): p. 2520-2534.
[36] Neese, F., *The ORCA program system.* Wiley Interdisciplinary Reviews: Computational Molecular Science, 2012. **2**(1): p. 73-78.
[37] Neese, F., *Software update: the ORCA program system, version 4.0.* Wiley Interdisciplinary Reviews: Computational Molecular Science, 2018. **8**(1).
[38] Adamo, C. and V. Barone, *Toward reliable density functional methods without adjustable parameters: The PBE0 model.* The Journal of Chemical Physics, 1999. **110**(13): p. 6158-6170.
[39] Weigend, F. and R. Ahlrichs, *Balanced basis sets of split valence, triple zeta valence and quadruple zeta valence quality for H to Rn: Design and assessment of accuracy.* Phys Chem Chem Phys, 2005. **7**(18): p. 3297-305.
[40] Grimme, S., et al., *A consistent and accurate ab initio parametrization of density functional dispersion correction (DFT-D) for the 94 elements H-Pu.* J Chem Phys, 2010. **132**(15): p. 154104.
[41] Grimme, S., S. Ehrlich, and L. Goerigk, *Effect of the damping function in dispersion corrected density functional theory.* J Comput Chem, 2011. **32**(7): p. 1456-65.
[42] Neese, F., *An improvement of the resolution of the identity approximation for the formation of the Coulomb matrix.* J Comput Chem, 2003. **24**(14): p. 1740-7.
[43] Weigend, F., *Accurate Coulomb-fitting basis sets for H to Rn.* Phys Chem Chem Phys, 2006. **8**(9): p. 1057-65.
[44] Neese, F., et al., *Efficient, approximate and parallel Hartree–Fock and hybrid DFT calculations. A 'chain-of-spheres' algorithm for the Hartree–Fock exchange.* Chemical Physics, 2009. **356**(1-3): p. 98-109.
[45] Riplinger, C. and F. Neese, *An efficient and near linear scaling pair natural orbital based local coupled cluster method.* J Chem Phys, 2013. **138**(3): p. 034106.
[46] Riplinger, C., et al., *Natural triple excitations in local coupled cluster calculations with pair natural orbitals.* J Chem Phys, 2013. **139**(13): p. 134101.
[47] Riplinger, C., et al., *Sparse maps--A systematic infrastructure for reduced-scaling electronic structure methods. II. Linear scaling domain based pair natural orbital coupled cluster theory.* J Chem Phys, 2016. **144**(2): p. 024109.

[48] Saitow, M., et al., *A new near-linear scaling, efficient and accurate, open-shell domain-based local pair natural orbital coupled cluster singles and doubles theory.* J Chem Phys, 2017. **146**(16): p. 164105.
[49] Guo, Y., et al., *Communication: An improved linear scaling perturbative triples correction for the domain based local pair-natural orbital based singles and doubles coupled cluster method [DLPNO-CCSD(T)].* J Chem Phys, 2018. **148**(1): p. 011101.
[50] Reiher, M., *Douglas-Kroll-Hess Theory: a relativistic electrons-only theory for chemistry.* Theoretical Chemistry Accounts, 2006. **116**(1-3): p. 241-252.
[51] Reiher, M. and A. Wolf, *Exact decoupling of the Dirac Hamiltonian. II. The generalized Douglas-Kroll-Hess transformation up to arbitrary order.* J Chem Phys, 2004. **121**(22): p. 10945-56.
[52] Wolf, A., M. Reiher, and B.A. Hess, *The generalized Douglas-Kroll transformation.* Journal of Chemical Physics, 2002. **117**(20): p. 9215-9226.
[53] van Wullen, C., *Relation between different variants of the generalized Douglas-Kroll transformation through sixth order.* J Chem Phys, 2004. **120**(16): p. 7307-13.
[54] Reiher, M., *Relativistic Douglas-Kroll-Hess theory.* Wiley Interdisciplinary Reviews-Computational Molecular Science, 2012. **2**(1): p. 139-149.
[55] Nakajima, T. and K. Hirao, *The higher-order Douglas-Kroll transformation.* Journal of Chemical Physics, 2000. **113**(18): p. 7786-7789.
[56] Douglas, M. and N.M. Kroll, *Quantum electrodynamical corrections to the fine structure of helium.* Annals of Physics, 1974. **82**(1): p. 89-155.
[57] Rolfes, J.D., F. Neese, and D.A. Pantazis, *All-electron scalar relativistic basis sets for the elements Rb-Xe.* J Comput Chem, 2020. **41**(20): p. 1842-1849.
[58] Pantazis, D.A., et al., *All-Electron Scalar Relativistic Basis Sets for Third-Row Transition Metal Atoms.* J Chem Theory Comput, 2008. **4**(6): p. 908-19.
[59] Stoychev, G.L., A.A. Auer, and F. Neese, *Automatic Generation of Auxiliary Basis Sets.* J Chem Theory Comput, 2017. **13**(2): p. 554-562.
[60] Barone, V. and M. Cossi, *Quantum calculation of molecular energies and energy gradients in solution by a conductor solvent model.* Journal of Physical Chemistry A, 1998. **102**(11): p. 1995-2001.
[61] Hanwell, M.D., et al., *Avogadro: an advanced semantic chemical editor, visualization, and analysis platform.* J Cheminform, 2012. **4**(1): p. 17.

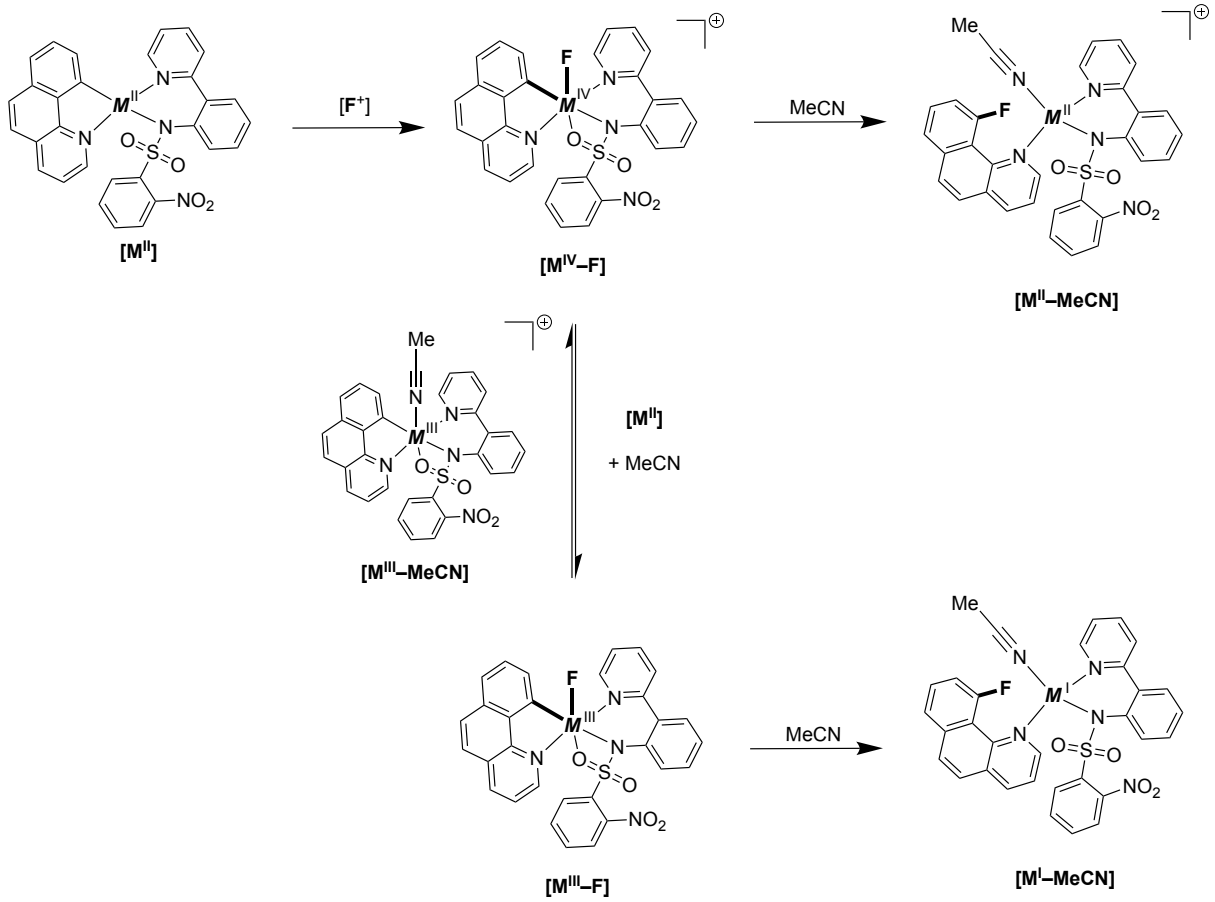

Fig. 1: Reaction system under consideration with ***M*** = **Ni**, **Pd**, **Pt**. The bonds involved in the reductive elimination reaction are highlighted.

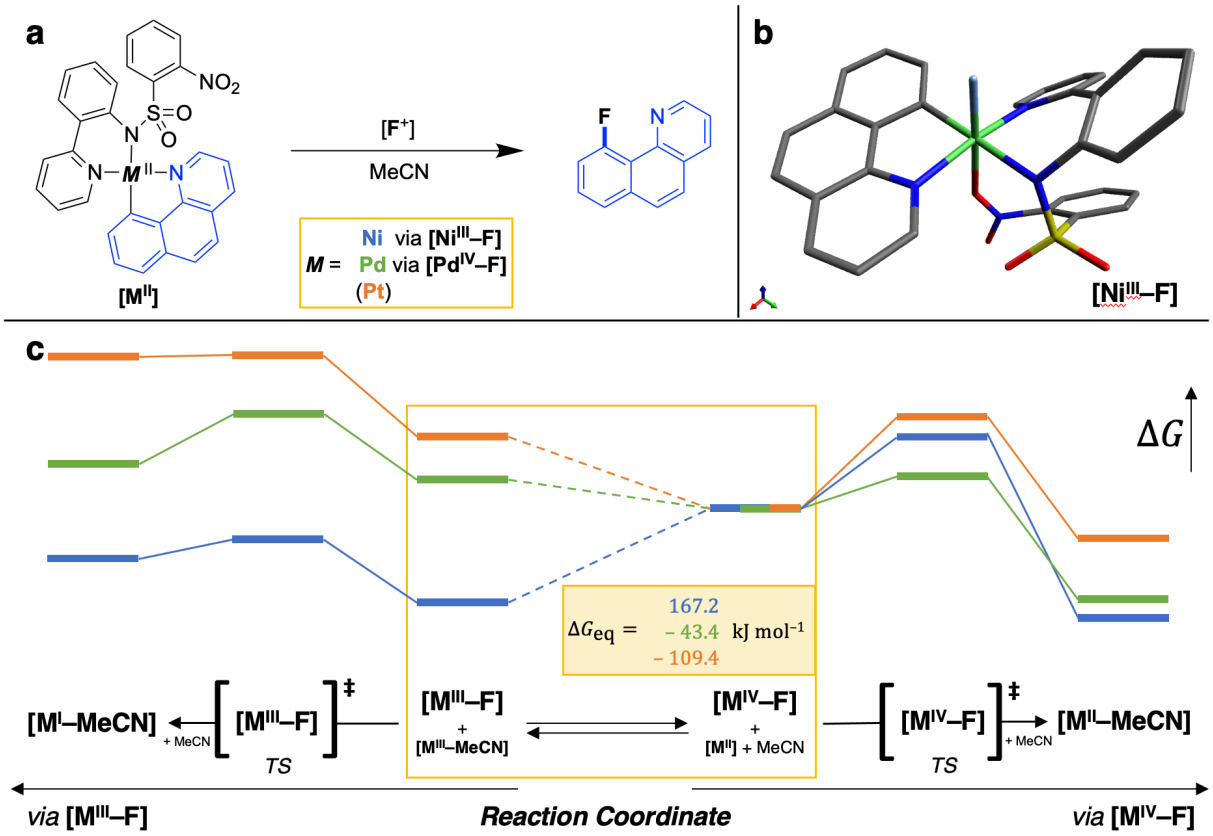

Fig. 2: a: Reductive elimination reaction under consideration with the active intermediates reported by Ritter et al.; **b**: Representative structure of [**Ni**$^{\mathbf{III}}$**–F**] active intermediate; **c**: Results of the potential energy surface analysis of the reaction system shown in Fig. 1.

Table 1: Key Gibbs Free Energies and activation barriers of the reaction system shown in Fig. 1, as depicted in Fig. 2c, and equilibrium constants K_{eq} of the central equilibrium:

Reaction	**Ni** [kJ/mol]	**Pd** [kJ/mol]	**Pt** [kJ/mol]
$\mathbf{\Delta G_{eq}}$	167.2	– 43.4	– 109.4
$\mathbf{K_{eq}}$	$1.62 \cdot 10^{-30}$	$5.41 \cdot 10^{7}$	$3.11 \cdot 10^{19}$
$\mathbf{\Delta G^{\ddagger}}$ **[M(III)–F]**	109.2	114.5	145.4
$\mathbf{\Delta G_{Red.El.}}$ **[M(III)–F]**	75.0	25.8	131.2
$\mathbf{\Delta G^{\ddagger}}$ **[M(IV)–F]**	118.2	51.4	165.9
$\mathbf{\Delta G_{Red.El.}}$ **[M(IV)–F]**	– 181.7	– 157.6	– 53.4

Table 2: Calculated XES energies of the [valence]$d_{xy} \rightarrow 1s$ transition, with orbital determinations based on *Loewdin Reduced Orbital Population per MO* analysis for the active intermediates, with the energy difference between alpha and beta spin for the open-shell [$\mathbf{M^{III}}$–**F**] system.

n$d_{xy} \rightarrow 1s$	$E_{[M^{III}-F]}$ [eV]			$E_{[M^{IV}-F]}$ [eV]
M =	α	β	ΔE (β – α)	α/β
Ni (n = 3)	8246.544	8247.28	0.736	8247.068
Pd (n = 4)	24199.046	24199.082	0.036	24199.299
Pt (n = 5)	78092.715	78092.736	0.021	78093.258